RSC Advances

PAPER

View Article Online
View Journal | View Issue

Cite this: *RSC Adv.*, 2025, **15**, 38189

Comprehensive analysis of polymethoxyflavone metabolism in orange peel using an animal model

Jin-Pyo An, Xin Liu, Dongjoo Kim, Robert Madden and Yu Wang *

Polymethoxyflavones (PMFs) are a unique class of flavonoids naturally present without attached sugar molecules and with a lack of exposed hydroxyl groups. This structural difference results in higher bioavailability. This study investigated the metabolism and tissue distribution of PMFs following oral administration of orange peel extract to mice. Tissue samples were subsequently analyzed using liquid chromatography-mass spectrometry (LC-MS). Our findings indicate that PMFs are efficiently absorbed and distributed, with their accumulation patterns directly related to their chemical structures. Specifically, a less bulky A-ring structure was found to be crucial for PMF distribution in different tissues. The absence of a methoxy group at the C-5 position enhanced penetration into the brain, while the presence of methoxy groups near the hydrogen bond region (C-4/5) decreased the accumulation of hydroxylated PMFs in the liver. Based on key-ion filtering strategies, a total of 87 PMF metabolites, including demethylated forms and conjugates with glucuronate and sulfate were identified using UHPLC-Orbitrap-HRMS. This study is the first to report on the practical distribution of PMFs in various tissues after the administration of a natural orange peel extract.

Received 2nd May 2025
Accepted 3rd October 2025

DOI: 10.1039/d5ra03091a

rsc.li/rsc-advances

1. Introduction

Polymethoxyflavones (PMFs) are a class of flavonoids noted for their potent bioactivity, which includes anti-obesity, anti-inflammatory, anticancer, antinociceptive, and anti-dementia effects.[1–4] PMFs are dominant phytochemicals in orange peel, and some representative PMFs such as sinensetin, nobiletin, and tangeretin, are particularly effective at decreasing chronic inflammatory cytokines like tumor necrosis factor (TNF)-α and interleukin (IL)-6.[5] Specifically, 5-demethylnobiletin demonstrates significant anti-atherogenic effects by reducing oxidized low density lipoprotein (LDL) uptake and enhancing hepatic LDL receptor activity.[2] Additionally, the essential oil from Gannan navel oranges has been shown to exhibit anticancer effects against human lung and prostate cancer cells, while sweet orange peel extract can significantly down-regulate key inflammatory genes such as cyclooxygenase (COX)-2 and TNF-α in animal models.[6,7] These findings collectively highlighted the significant health benefits of PMFs and orange peel extract.

The bioavailability of PMFs is critical for their bioactivity, as it determines whether these compounds can reach target tissues to exert their beneficial effects.[8] The unique chemical structure of PMFs, particularly the methylation of hydroxyl groups, plays a key role in their high bioavailability. Unlike typical flavonoids that undergo rapid metabolism through glucuronidation or sulfation, the methylated hydroxyl groups in PMFs prevent these processes, leading to increased stability and bioavailability.[9,10] *In vitro* and *in vivo* studies have confirmed this, showing that methylated derivatives exhibit greater metabolic stability and higher concentrations in plasma and tissues compared to their non-methylated counterparts.[11,12] Beyond methylation, the three-dimensional structure of PMFs also enhances their bioavailability. The carbon double bond between C-2 and C-3 in the C-ring results in a more planar and stable structure. This planar conformation, along with reduced polarity and optimal molecular size, allows PMFs to be efficiently transported across biological membranes, further contributing to their high bioavailability.[13]

So far, several studies have examined PMF bioavailability, most have focused on administering one or two single compounds. For example, sinensetin and its metabolites have been detected in plasma, urine, and feces of rats, and the distribution of tangeretin in various rat tissues has been quantified.[14,15] Additionally, mono-demethylated metabolites of nobiletin have been analyzed after oral administration.[16] However, a comprehensive study using a complete orange peel extract, which contains the full spectrum of PMFs, has not been conducted to determine tissue distribution. Our present study is aimed at addressing this gap by administering orange peel extract to mice and analyzing its distribution across a wide range of tissues, including plasma, urine, feces, liver, kidneys, brain, testes, small intestine, and colon. The accumulation levels of the original PMFs in different tissues were quantified using a triple quadrupole liquid chromatography-mass

Food Science and Human Nutrition, Citrus Research and Education Center, University of Florida, 700 Experiment Station Road, Lake Alfred, FL 33850, USA. E-mail: yu.wang@ufl.edu

spectrometry (LC-MS), and these accumulation levels were correlated with their structural properties as well. Furthermore, metabolized PMFs based on key-ion patterns were identified using a UHPLC-Orbitrap-high resolution (HR)MS. Our previous research, which involved isolating individual PMF compounds, enabled us to not only quantify these compounds but also obtain empirical key-ions for their identification.[17] This study provides a comprehensive analysis of PMF absorption and tissue-specific distribution, offering critical insights into their metabolism and potential health benefits.

2. Experimental

2.1. Chemicals and reagents

Acetonitrile, methanol, water, and formic acid of LC-MS grade were obtained from Fisher Scientific (Fair Lawn, NJ, USA), while taxifolin was sourced from Sigma-Aldrich (St. Louis, MO, USA).

2.2. Animal treatment and sample preparation

Animal treatment was performed as described in a previous study, with all procedures receiving approval from the Institutional Animal Care and Use Committee at the Western Regional Research Center, USDA, Albany, CA, USA (protocol no. IACUC202200000487).[18] Male C57BL/6 mice, 6 weeks of age and approximately 22 g, were purchased from Jackson Laboratory (Bar Harbor, ME, USA). Upon arrival, the mice were housed individually in a controlled environment with a 12-hour light/dark cycle, maintained at a room temperature of approximately 25 °C and 70% humidity. Following a one-week acclimation period, during which they had free access to a standard chow diet (LabDiet #5015, PMI International, Redwood City, CA, USA) and drinking water ad libitum, the mice were randomized into experimental groups, and the feeding protocols were initiated when the mice were 7 weeks old. Customized diets containing orange peel extract were sourced from Envigo (Madison, WI), where the extract was added to a high-fat base diet (Teklad 2918) at a concentration of 10 mg g^{-1}. Mice in the experimental group were fed a high-fat diet consisting of 1% w/w orange peel extract combined with 0.65% carnitine in their drinking water, while the control group received a high-fat diet with 0.65% carnitine in their drinking water. Throughout the 6-week feeding period, all mice had *ad libitum* access to food and water. At the conclusion of the study, urine samples were collected directly from the cage floor and immediately stored at −80 °C for further analysis. Blood was collected *via* cardiac puncture using syringes pre-rinsed with EDTA. Plasma was then separated by centrifugation at 2000×*g* for 15 min and subsequently stored at −80 °C. Various tissues, including brain, liver, small intestine mucosa, colon mucosa, testes, and kidney, were excised and rinsed with saline. Tissues were homogenized under liquid nitrogen using a mortar and pestle, then extracted with methanol containing 0.1% of dimethyl sulfoxide (DMSO). Plasma or urine (20 μL) was extracted with 200 μL of methanol containing 0.1% DMSO. After centrifugation at 10 000×*g* for 10 min at 4 °C, the supernatants were filtered through a 0.2 μm nylon filter prior to LC analysis. Taxifolin was added as an internal standard.

2.3. Preparation of compound and key-ion filtering

A total of 11 compounds were isolated from orange peel, and their structures were determined using nuclear magnetic resonance (NMR) spectroscopy, as described in a previous study.[17] These include 6,7,8,3′,4′-pentamethoxyflavone (**1**), 3,6,7,8,2′,5′-hexamethoxyflavone (**2**), nobiletin (**3**), 5,6,7,4′-tetramethoxyflavone (**4**), 3,5,6,7,8,3′,4′-heptamethoxyflavone (**5**), tangeretin (**6**), 3-methoxytangeretin (**7**), 5-hydroxy-6,7,8,3′,4′-pentamethoxyflavone (**8**), 5-hydroxy-3,7,8,3′,4′-pentamethoxyflavone (**9**), sinensetin (**10**), 5-hydroxy-3,6,7,8,3′,4′-hexamethoxyflavone (**11**) (Fig. S1). Each isolated compound was analyzed using high-resolution Orbitrap mass spectrometry to determine its key-ions (Table 1). Fig. 1 exemplifies the plausible mass fragmentation pathway of tangeretin and its corresponding key-ions.

2.4. Quantification of PMFs using triple quadrupole tandem mass spectrometry

LC–MS/MS analysis was performed using an Ultimate 3000 LC system coupled to a TSQ Quantiva triple quadrupole mass spectrometer (Thermo Fisher Scientific, San Jose, CA, USA). Analytes were separated on a Thermo Acclaim C 30 chromatography column (2.1 × 150 mm, 3.0 μm) with the column temperature at 40 °C. The mobile phases consisted of 0.1% formic acid in water (A) and 0.1% formic acid in acetonitrile (B). The gradient elution profile was as follows: 0–4 min 20% B, 4–29 min 20–80% B, and 29–35 min 100% B, followed by a 5 min re-equilibration. The flow rate was maintained at 0.25 mL min^{-1}, and the injection volume was 4 μL. An electrospray ionization (ESI) source in positive ion mode was used. The ESI settings were as follows: spray voltage, 3500 V; ion transfer tube temperature, 325 °C; vaporizer temperature, 300 °C; and sheath, auxiliary, and sweep gas flows set at 40, 12, and 1 Arb, respectively. MS/MS detection was conducted in selective reaction monitoring (SRM) mode, with optimal parameters for each PMF compound listed in Table S1. Data processing and instrument control were managed using Xcalibur 3.0.

2.5. Method validation

To validate our proposed method, we examined various metrics including linearity, limit of detection (LOD), limit of quantification (LOQ), precision, and recovery. The linearity, LOD, and LOQ of each compound are listed in Table S2. All compounds demonstrated good linearity (R^2 > 0.999) across the concentration ranges. The LOD was defined as the concentration with a signal-to-noise (S/N) ratio of 3.3, while the LOQ corresponded to a S/N ratio of 10. To assess precision, three different concentrations from the linear range of the calibration curve were analyzed for each test compound. Intra-day precision was evaluated by analyzing each concentration in triplicate on the same day. Inter-day precision was determined by analyzing three replicates of each concentration over three consecutive days. The results, summarized in Table S3, showed that the

Table 1 Key-ions of each PMF compound

Compound	t_R (min)	Calculated Mass (m/z) $[M + H]^+$	Chemical formula $[M + H]^+$	Key-ions
1	20.21	373.1287	$C_{20}H_{21}O_7$	315.0866, 312.0986, 311.0904, 296.0677, 283.0961, 268.0725, 199.0235, 181.0127, 163.0752, 153.0181, 151.0388, 121.0279
2	20.73	403.1392	$C_{21}H_{23}O_8$	315.0503, 313.0705, 301.0705, 299.0913, 277.0704, 259.0595, 231.0652, 229.0338, 211.0236, 193.0128, 183.0287, 165.0545
3	21.12	403.1392	$C_{21}H_{23}O_8$	313.0167, 309.2051, 303.1053, 302.1019, 298.2738, 293.2105, 286.1070, 255.1954, 251.1640, 203.1792, 191.1426, 169.1770
4	21.32	343.1181	$C_{19}H_{19}O_6$	313.0705, 309.0754, 297.0757, 281.0807, 267.0650, 239.0701, 199.0235, 181.0130, 153.0181, 133.0647
5	21.60	433.1498	$C_{22}H_{25}O_9$	327.0084, 285.0636, 241.2157, 237.1843, 233.2055, 219.1743, 168.1380, 151.1116, 137.1323
6	22.00	373.1287	$C_{20}H_{21}O_7$	315.0857, 313.0707, 311.0895, 283.0957, 211.0237, 183.0288, 161.0596, 159.0446, 132.0570
7	22.41	403.1392	$C_{21}H_{23}O_8$	315.0502, 311.0547, 301.0693, 287.0547, 269.0439, 259.0601, 241.0494, 229.0337, 211.0240, 183.0289
8	22.77	389.1236	$C_{20}H_{21}O_8$	302.3052, 299.2579, 295.1902, 286.3102, 275.5783, 263.0513, 235.1692, 211.0600, 183.0651, 171.1489, 138.0313, 127.0388
9	23.62	389.1236	$C_{20}H_{21}O_8$	327.0080, 317.1722, 315.1226, 299.2580, 295.1903, 283.2532, 281.1474, 263.0514, 235.1692, 229.1958, 171.1489, 149.0596
10	20.41	373.1287	$C_{20}H_{21}O_7$	315.0766, 313.0688, 299.0449, 283.0534, 255.0537, 231.0186, 223.0691, 218.7799, 174.8372, 141.0942, 133.0436
11	24.13	419.1342	$C_{21}H_{23}O_9$	315.7474, 310.5835, 291.0862, 279.0754, 278.0565, 270.0699, 230.2474, 224.4033, 205.4430, 171.1489, 165.0545, 153.1272

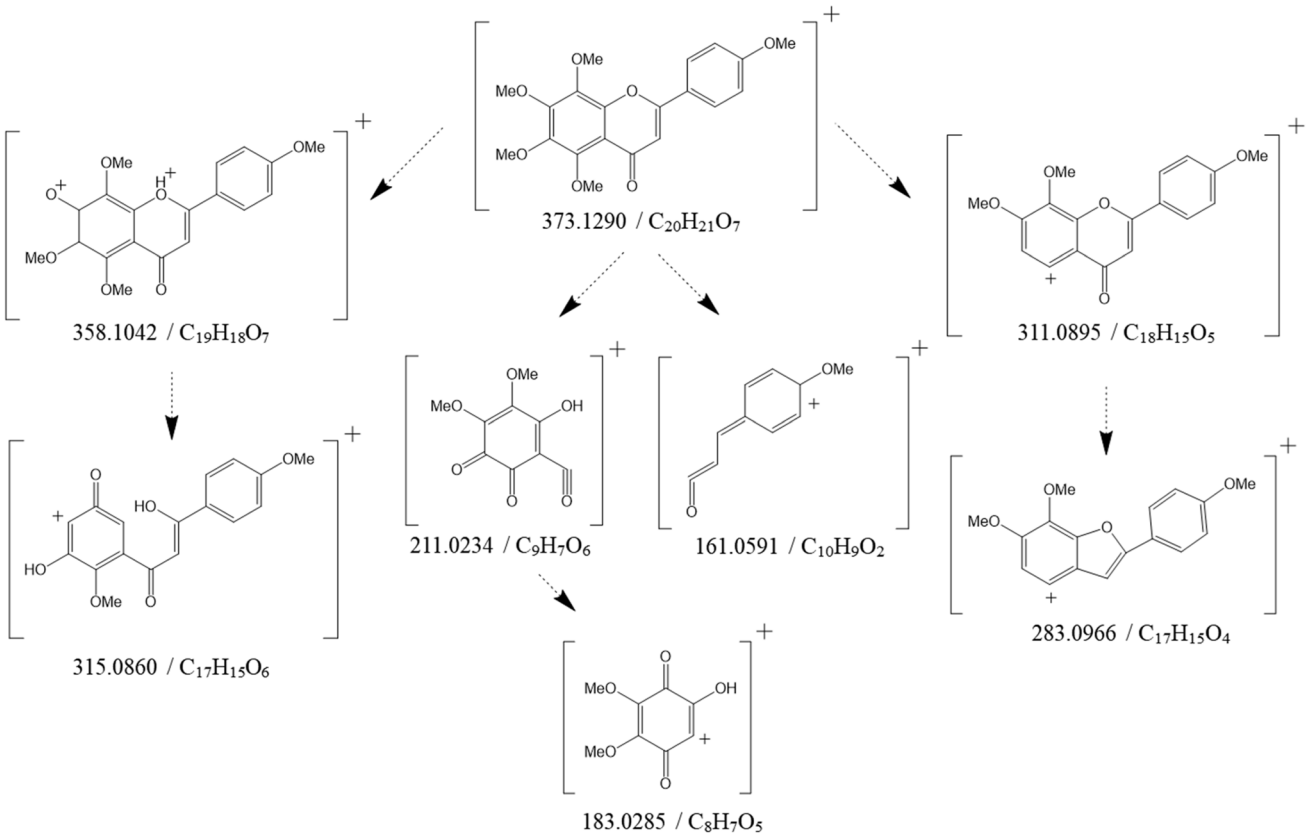

Fig. 1 Plausible fragment pathway of tangeretin. Mass fragmentation was generated by HRMS in ESI positive mode. The top of the figure shows the parent compound, tangeretin, with a molecular mass of 373.1290, followed by detailed fragmented structures below.

relative standard deviation (RSD) values for both intra- and inter-day precision were below 7.9%, which met the acceptable criteria for accuracy and precision. This confirms that our method is reliable and reproducible for the quantitative analysis of PMFs. Extraction recovery was determined by comparing the response of PMFs in tissue extracts to the response of an identical concentration of analyte added to solutions extracted from blank tissues. As shown in Table S4, the recovery rates were between 85% and 110% at all concentrations.

2.6. Identification of metabolites using high resolution mass spectrometry

The UHPLC separation was performed on a Thermo Vanquish Flex Binary RSLC platform using an Agilent C30 chromatography column (2.1 × 150 mm, 3.0 μm) with a column temperature maintained at 40 °C. The mobile phases consisted of 0.1% formic acid in water (A) and 0.1% formic acid in acetonitrile (B). The gradient profile was as follows: 0–3 min 2% B, 3–29 min 2–90% B, 29–30 min 90–100% B, and 30–35 min 100% B. The column was re-equilibrated for 5 min with the initial mobile phase composition. The flow rate was set at 0.2 mL min^{-1}, and the injection volume was 3 μL. MS detection was conducted using a Q-Exactive-Orbitrap mass spectrometry. The instrument's resolution was set to 140 000 based on empirical data. Automated gain control (AGC) was configured at 3×10^6, with a maximum ion accumulation time (IT) of 600 ms. In the MS^2 experiment, the stepped normalized collision energy (NCE) was set at 20, 40, and 60 eV, with a resolution set at 17 500. The *m*/*z* range was maintained as in the full MS experiment. The AGC was set to 1×10^3, and the IT was 50 ms. Data-dependent analysis (DDA) was employed to initiate the second-stage fragmentation, targeting the 12 parent ions with the highest intensity during each MS^1 scan for further MS^2 fragmentation. Additional parameters are described in Table S5.

3. Results and discussion

PMFs are increasingly recognized for their health benefits, making it crucial to understand how they are absorbed, distributed, and metabolized to optimize their therapeutic potential.[15,19] By clarifying how PMFs are distributed throughout the body, researchers can ensure that optimal concentrations reach targeted sites, thereby improving their efficacy.[20] However, current information on the distribution and metabolism of PMFs remains limited. We analyzed 11 different PMFs in this experiment, categorizing them into three groups: five major non-hydroxylated PMFs including 6,7,8,3′,4′-pentamethoxyflavone (PMF **1**), nobiletin (PMF **3**), 5,6,7,4′-tetramethoxyflavone (PMF **4**), 3,5,6,7,8,3′,4′-heptamethoxyflavone (PMF **5**), and tangeretin (PMF **6**); three minor non-hydroxylated PMFs including 3,6,7,8,2′,5′-hexamethoxyflavone (PMF **2**), 3-

methoxytangeretin (PMF 7), and sinensetin (PMF **10**); and three hydroxylated PMFs, including 5-hydroxy-6,7,8,3′,4′-pentamethoxyflavone (PMF **8**), 5-hydroxy-3,7,8,3′,4′-pentamethoxyflavone (PMF **9**), and 5-hydroxy-3,6,7,8,3′,4′-hexamethoxyflavone (PMF **11**). The contents of major non-hydroxylated PMFs in orange peel exceeded 15 000 ppm, while those minor non-hydroxylated PMFs were present at less than 2000 ppm. We measured the levels of 11 PMFs in orange peel and different tissues such as plasma, urine, feces, testes, brain, colon, liver, kidneys, and small intestine. Their values are listed in Table S6 and depicted in a pie chart in Fig. S2. To better understand the tissue-specific accumulation of PMFs, we calculated the tissue-peel ratio for each compound. This was done by dividing the PMF content into a specific tissue by its content in the orange peel (as shown in Fig. 2 and Table 2). This ratio allowed us to account for the varying original concentrations of each PMF and determine which chemical structures accumulate preferentially in certain tissues.

3.1. Plasma

In this study, only five major non-hydroxylated PMFs (**1**, **3**, **4**, **5**, and **6**) were detected in plasma. Minor non-hydroxylated PMFs or hydroxylated PMFs were not found. Hydroxylated PMFs might have undergone rapid conjugation with glucuronate or sulfate, which are common metabolic pathways for hydroxyl groups, leading to their swift clearance from bloodstream.[21–23]

As shown in Table 2, PMF **3** had the highest plasma-peel ratio, while PMF **1** had the lowest. The key structural difference between these two compounds is that PMF **3** contains one more methoxy group at the C-5 position, which is absent in PMF **1**. The presence of methoxy at this position has been reported to increase the maximum absorption (C_{max}) and the area under the curve (AUC_{last}). Therefore, the higher accumulation of PMF **3** in plasma compared to PMF **1** may be attributed to the presence of its C-5 methoxy group. The plasma-peel ratios of PMF **3** and PMF **5** suggested functional role for the methoxy group at the C-3 position. The key difference is that PMF **5** contains a methoxy group at C-3, which is absent in PMF **3**. This methoxy group has been shown to increase the C_{max} and AUC_{last}, but decrease the time to maximum concentration (T_{max}). As a result, PMF **5** likely had a lower T_{max} value than PMF **3**. Given that the mice were sacrificed 12 h after food intake, a point when PMF concentrations are known to decrease after an initial high within the first 4 hours, it is likely that PMF **5**'s concentration had already peaked and declined.[23] In contrast, PMF **3**, with a higher T_{max} value, may have still been present in higher concentrations in plasma at the time of sacrifice. Additionally, the higher content of PMF **3** could be attributed to enterohepatic recirculation.

3.2. Urine and feces

In this study, the content of parent PMFs in feces was significantly higher than that in urine. This is likely due to the lipophilicity and relatively large molecular size of PMFs, which favor their excretion *via* the fecal route. This finding is consistent with previous research on nobiletin and tangeretin.[13,14] Structural differences were found to affect accumulation, particularly for hydroxylated PMFs. As displayed in Table 2, the feces-peel ratio of PMF **8** was twice as high as that of PMF **11**, while their urine-peel ratio was similar. Structurally, PMF **11**

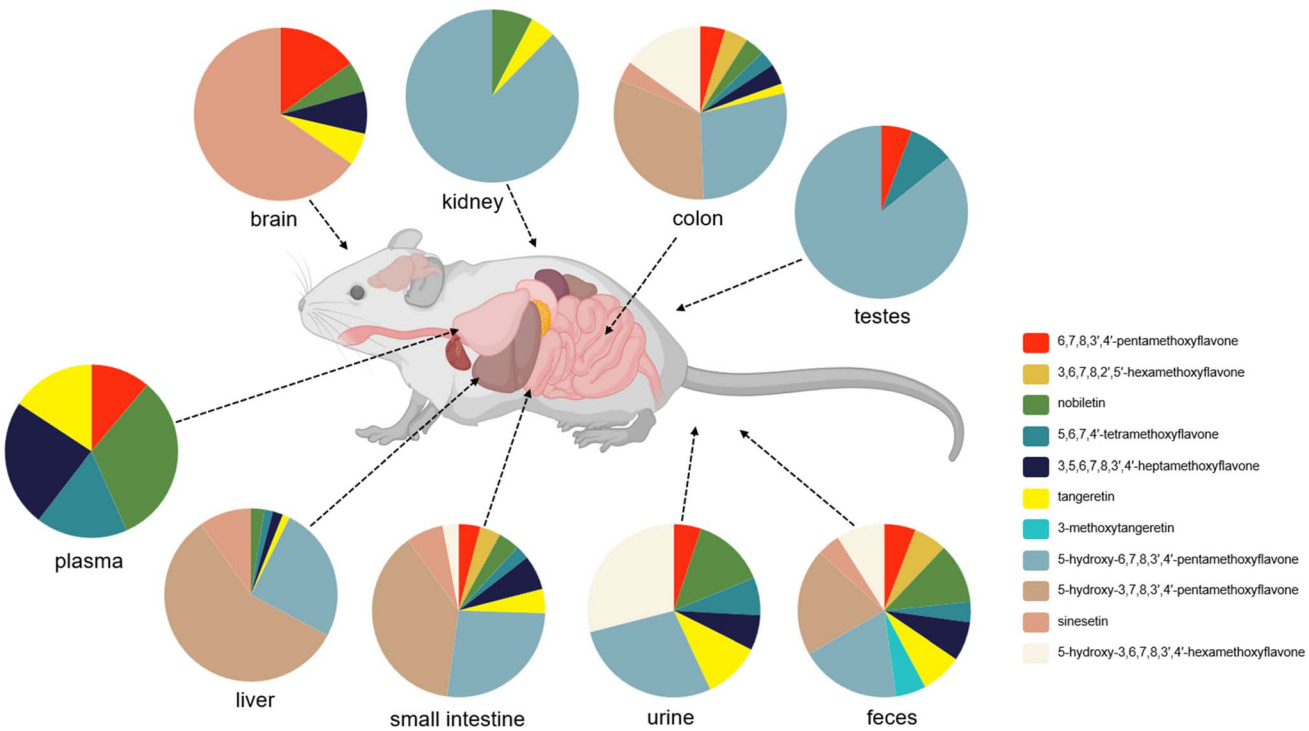

Fig. 2 Distribution of PMFs in various tissues following oral administration of orange peel extract. The area of the pie chart is calculated based on the tissue–peel ratio. Each color represents one of the 11 different PMFs, with names indicated on the right side of the chart.

Table 2 Tissue–peel ratio by dividing the content of each PMF in a specific tissue by its content in the orange peel[a]

Compound	Urine	Feces	Plasma	Small intestine	Liver	Brain	Testes	Colon	Kidney
1	0.108	65.949	0.030	2.697		0.036	0.016	0.314	
2		69.555		2.535				0.294	
3	0.279	126.886	0.086	2.653	0.055	0.014		0.248	0.021
4	0.149	42.769	0.046	1.676	0.035		0.023	0.198	
5	0.139	81.722	0.064	4.286	0.042	0.019		0.258	
6	0.226	86.216	0.042	2.978	0.030	0.015		0.121	0.013
7		63.616							
8	0.591	211.794		17.594	0.558		0.234	1.890	0.238
9		224.300		25.017	1.260			2.134	
10		48.738		4.608	0.216	0.159		0.254	
11	0.614	100.872		1.951				1.014	

[a] Tissue–peel ratio value was calculated as follows; (dividing the content of each PMF in a specific tissue by its content in the orange peel) × 1000 × 100. The factor of 1000 was used because the concentration unit of the orange peel (ppm) is 1000 times higher than that of the tissue. The factor of 100 was used to obtain a percentage.

contains a methoxy group at C-3 position, which is absent in PMF **8**. This suggested that a C-3 methoxy group might increase fecal accumulation. Similarly, PMF **9**, another hydroxylated PMF with a C-3 methoxy group, showed the highest feces-to-peel ratio among all PMFs. The unique chemical feature of PMF **9** is the absence of a methoxy group at C-6 position, which could also influence its fecal accumulation ratio. Notably, metabolized PMFs were most commonly found in urine and feces, in addition to parent compounds.[24] These findings may contribute to a better structural understanding of PMF bioavailability as it relates to excretion in urine and feces.

3.3. Testes

In this study, two major PMFs **1** and **4** and one hydroxylated PMF **8** were detected in the testes. Interestingly, the two major detected PMFs **1** and **4** have A-rings that are not fully substituted with methoxy groups, while the other three major PMFs **3**, **5**, and **6** that were not detected are fully substituted at the C-5,6,7,8 position. Furthermore, hydroxylated PMF **8** showed a testes-to-peel ratio that was 10 to 14 times higher than that of the detected major PMFs **1** and **4**, seen in Table 2. These findings are significant for identifying effective nutraceuticals for testicular delivery, as the blood-testis barrier (BTB) makes it difficult for many phytochemicals to reach the testes.[25] Our results suggest that PMFs with a less bulky A-ring structure and certain hydroxylated forms are more efficient at penetrating this barrier.

3.4. Brain

As shown in Table 2, PMFs **1**, **3**, **5**, **6**, and **10** were found in the brain. PMFs **1** and **10** exhibited a higher brain-peel ratio compared to the other compounds. A key structural feature of these two PMFs is a less bulky A-ring, as they lack a methoxy group at the C-5 and C-7 positions, respectively. This less substituted A-ring structure may facilitate more efficient penetration of the blood–brain barrier (BBB). Previous studies demonstrated that oral administration of nobiletin for four weeks was found to prevent spatial learning impairments induced by Aβ1-42, as evaluated in a Morris water maze test. Additionally, nobiletin enhanced acetylcholinesterase activity in both the cortex and hippocampus.[26] The administration of the hydroxylated polymethoxyflavone, 4′-demethylnobiletin, has been shown to alleviate learning impairments associated with *N*-methyl-D-aspartate receptor antagonism. This compound was also detected in the brain following intraperitoneal administration.[27] However, hydroxylated PMFs (**8**, **9**, and **11**) were not detected in the brain in our study. This discrepancy may be attributed to two key factors, (1) chemical structure: the hydroxylated PMFs in our study contain a hydroxyl group on the A-ring (at C-5), unlike 4′-demethylnobiletin, which has a hydroxyl group on the B-ring (at C-4′). The C-5 hydroxyl group can form an intramolecular hydrogen bond with the C-4 ketone group, which may significantly alter the compound's physicochemical properties and its ability to cross BBB; (2) administration method: the previous study used intraperitoneal administration, whereas our study used oral administration. The oral route exposes compounds to first-pass metabolism in liver, which could lead to a lower bioavailability and thus, a reduced concentration of PMFs reaching the brain.

3.5. Colon

The colon is a vital part of the digestive system, hosting a complex community of gut microbiota that aids in fermenting food residues and supporting immune function.[28] PMFs are noted for their bioactive properties in the colon. A study by Zhang *et al.* demonstrated that after 11 weeks of treatment, aged citrus peel (chenpi) extract significantly enhanced the growth of *Lactobacillus* and *Bifidobacterium*, showcasing a notable prebiotic effect.[29] Additionally, a PMF-rich fraction from Ougan fruit has been shown to dynamically modulate *Akkermansia* populations in a dose- and time-dependent manner.[30] Our research group has also demonstrated that orange peel increased the levels of beneficial probiotics.[17]

In this study, all PMFs, except for PMF **7**, were detected in the colon. Overall, hydroxylated PMFs had a significantly higher colon-peel ratio compared to non-hydroxylated PMFs. Among the non-hydroxylated PMFs, PMFs **1** and **2** showed the highest

Table 3 Metabolite profiling in various tissues. (U: urine, F: feces, P: plasma, S: small intestine, L: liver, C: colon, K: kidney T: testes, B: brain)

Metabolite	t_R (min)	Chemical formula	Chemical formula	Observed Mass (m/z)	Mass error (ppm)	Identification	Detected tissue
M1	11.95	497.0753 $[M-H]^-$	$C_{21}H_{21}SO_{12}$	497.0762 $[M-H]^-$	1.81	Demethylation & sulfation of PMF **5**	U, F, L
M2	13.36	497.0753 $[M-H]^-$	$C_{21}H_{21}SO_{12}$	497.0762 $[M-H]^-$	1.81	Demethylation & sulfation of PMF **5**	U, F, L
M3	14.12	453.0491 $[M-H]^-$	$C_{19}H_{17}SO_{11}$	453.0496 $[M-H]^-$	1.103	Demethylation & sulfation of PMF **8**	U, F
M4	14.19	497.0753 $[M-H]^-$	$C_{21}H_{21}SO_{12}$	497.0758 $[M-H]^-$	1.005	Demethylation & sulfation of PMF **5**	U
M5	14.25	453.0491 $[M-H]^-$	$C_{19}H_{17}SO_{11}$	453.0511 $[M-H]^-$	4.414	Demethylation & sulfation of PMF **8**	U
M6	14.56	505.1346 $[M+H]^+$	$C_{24}H_{25}O_{12}$	505.1338 $[M+H]^+$	−1.583	Demethylation & glucuronidation of PMF **4**	U, S, L
M7	14.79	581.1506 $[M+H]^+$	$C_{26}H_{29}O_{15}$	581.1498 $[M+H]^+$	−1.376	Demethylation & glucuronidation of PMF **11**	U, S
M8	14.89	535.1451 $[M+H]^+$	$C_{25}H_{27}O_{13}$	535.1446 $[M+H]^+$	−0.934	Demethylation & glucuronidation of PMF **10**	U, S, L, C
M9	15.04	551.1400 $[M+H]^+$	$C_{25}H_{27}O_{14}$	551.1390 $[M+H]^+$	−1.814	Demethylation & glucuronidation of PMF **8**	U, S
M10	15.09	565.1557 $[M+H]^+$	$C_{26}H_{29}O_{14}$	565.1547 $[M+H]^+$	−1.769	Demethylation & glucuronidation of PMF **3**	U, S, L, C
M11	15.12	535.1451 $[M+H]^+$	$C_{25}H_{27}O_{13}$	535.1443 $[M+H]^+$	−1.494	Demethylation & glucuronidation of PMF **6**	U, S, L, C
M12	15.3	505.1346 $[M+H]^+$	$C_{24}H_{25}O_{12}$	505.1338 $[M+H]^+$	−1.583	Demethylation & glucuronidation of PMF **4**	U, F, P, S, L, C, K
M13	15.41	551.1400 $[M+H]^+$	$C_{25}H_{27}O_{14}$	551.1392 $[M+H]^+$	−1.451	Demethylation & glucuronidation of PMF **8**	U, S
M14	15.53	535.1451 $[M+H]^+$	$C_{25}H_{27}O_{13}$	535.1443 $[M+H]^+$	−1.494	Demethylation & glucuronidation of PMF **1**	U, F, P, S, L, C, K
M15	15.65	551.1400 $[M+H]^+$	$C_{25}H_{27}O_{14}$	551.1392 $[M+H]^+$	−1.451	Demethylation & glucuronidation of PMF **8**	U, F
M16	15.69	505.1346 $[M+H]^+$	$C_{24}H_{25}O_{12}$	505.1336 $[M+H]^+$	−1.979	Demethylation & glucuronidation of PMF **4**	U, P
M17	15.71	565.1557 $[M+H]^+$	$C_{26}H_{29}O_{14}$	565.1547 $[M+H]^+$	−1.769	Demethylation & glucuronidation of PMF **3**	U, S, L, C, K
M18	15.74	407.0436 $[M-H]^-$	$C_{18}H_{15}SO_9$	407.0442 $[M-H]^-$	1.474	Demethylation & sulfation of PMF **4**	U, F, L
M19	15.86	565.1557 $[M+H]^+$	$C_{26}H_{29}O_{14}$	565.1549 $[M+H]^+$	−1.415	Demethylation & glucuronidation of PMF **3**	U, F, P, S, L, C, K
M20	15.89	581.1506 $[M+H]^+$	$C_{26}H_{29}O_{15}$	581.1498 $[M+H]^+$	−1.376	Demethylation & glucuronidation of PMF **11**	U, S, C, K
M21	15.92	535.1451 $[M+H]^+$	$C_{25}H_{27}O_{13}$	535.1443 $[M+H]^+$	−1.494	Demethylation & glucuronidation of PMF **6**	U, F, P, S, L, C, K
M22	16.05	467.048 $[M-H]^-$	$C_{20}H_{19}SO_{11}$	467.0650 $[M-H]^-$	−0.642	Demethylation & sulfation of PMF **3**	F, L
M23	16.09	595.1663 $[M+H]^+$	$C_{27}H_{31}O_{15}$	595.1655 $[M+H]^+$	−1.344	Demethylation & glucuronidation of PMF **5**	U, S
M24	16.12	551.1400 $[M+H]^+$	$C_{25}H_{27}O_{14}$	551.1394 $[M+H]^+$	−1.088	Demethylation & glucuronidation of PMF **8**	U, S, C
M25	16.15	565.1557 $[M+H]^+$	$C_{26}H_{29}O_{14}$	565.1548 $[M+H]^+$	−1.592	Demethylation & glucuronidation of PMF **3**	U, F, P, S, L, C, K
M26	16.2	535.1451 $[M+H]^+$	$C_{25}H_{27}O_{13}$	535.1447 $[M+H]^+$	−0.747	Demethylation & glucuronidation of PMF **6**	L
M27	16.24	551.1400 $[M+H]^+$	$C_{25}H_{27}O_{14}$	551.1393 $[M+H]^+$	−1.27	Demethylation & glucuronidation of PMF **8**	U, S
M28	16.45	595.1663 $[M+H]^+$	$C_{27}H_{31}O_{15}$	595.1655 $[M+H]^+$	−1.344	Demethylation & glucuronidation of PMF **5**	U, F, P, S, L, C, K
M29	16.54	407.0436 $[M-H]^-$	$C_{18}H_{15}SO_9$	407.0442 $[M-H]-$	1.474	Demethylation & sulfation of PMF **4**	U, F, S, L, C, K
M30	16.6	437.0542 $[M-H]^-$	$C_{19}H_{17}SO_{10}$	437.0546 $[M-H]^-$	0.915	Demethylation & sulfation of PMF **6**	U, F, S, L, C, K
M31	16.69	375.1079 $[M+H]^+$	$C_{19}H_{19}O_8$	375.1075 $[M+H]^+$	−1.066	Demethylation of PMF **8**	U, F, C, T
M32	16.72	581.1506 $[M+H]^+$	$C_{26}H_{29}O_{15}$	581.1499 $[M+H]^+$	−1.204	Demethylation & glucuronidation of PMF **11**	U, S
M33	16.8	407.0436 $[M-H]^-$	$C_{18}H_{15}SO_9$	407.0440 $[M-H]^-$	0.982	Demethylation & sulfation of PMF **4**	U
M34	16.84	437.0542 $[M-H]^-$	$C_{19}H_{17}SO_{10}$	437.0543 $[M-H]^-$	0.228	Demethylation & sulfation of PMF **6**	U
M35	16.94	467.0648 $[M-H]^-$	$C_{20}H_{19}SO_{11}$	467.0649 $[M-H]^-$	0.214	Demethylation & sulfation of PMF **3**	U
M36	16.99	437.0542 $[M-H]^-$	$C_{19}H_{17}SO_{10}$	437.0542 $[M-H]^-$	0	Demethylation & sulfation of PMF **1**	U, F
M37	17.02	437.0541 $[M-H]^-$	$C_{19}H_{17}SO_{10}$	437.0544 $[M-H]^-$	0.457	Demethylation & sulfation of PMF **10**	U, F, S
M38	17.04	453.0491 $[M-H]^-$	$C_{19}H_{17}SO_{11}$	453.0497 $[M-H]^-$	1.324	Demethylation & sulfation of PMF **8**	U, F, S, L, C
M39	17.07	375.1079 $[M+H]^+$	$C_{19}H_{19}O_8$	375.1075 $[M+H]^+$	−1.066	Demethylation of PMF **8**	U, F, S, C, T
M40	17.11	359.1130 $[M+H]^+$	$C_{19}H_{19}O_7$	359.1127 $[M+H]^+$	−0.835	Demethylation of PMF **1**	U, F, P, S
M41	17.2	437.0542 $[M-H]^-$	$C_{19}H_{17}SO_{10}$	437.0545 $[M-H]^-$	0.686	Demethylation & sulfation of PMF **1**	U, F, S, L, C, K
M42	17.26	535.1451 $[M+H]^+$	$C_{25}H_{27}O_{13}$	535.1445 $[M+H]^+$	−1.121	Demethylation & glucuronidation of PMF **10**	U, S, L, C
M43	17.3	453.0491 $[M-H]^-$	$C_{19}H_{17}SO_{11}$	453.0498 $[M-H]^-$	1.545	Demethylation & sulfation of PMF **9**	U, F
M44	17.32	467.0648 $[M-H]^-$	$C_{20}H_{19}SO_{11}$	467.0650 $[M-H]^-$	0.428	Demethylation & sulfation of PMF **3**	U, F, S, L, C
M45	17.35	551.1400 $[M+H]^+$	$C_{25}H_{27}O_{14}$	551.1393 $[M+H]^+$	−1.27	Demethylation & glucuronidation of PMF **9**	U, S, L
M46	17.41	437.0542 $[M-H]^-$	$C_{19}H_{17}SO_{10}$	437.0542 $[M-H]^-$	0	Demethylation & sulfation of PMF **6**	U, F

Table 3 (*Contd.*)

Metabolite	t_R (min)	Chemical formula	Chemical formula	Observed Mass (m/z)	Mass error (ppm)	Identification	Detected tissue
M47	17.43	535.1451 $[M + H]^+$	$C_{25}H_{27}O_{13}$	535.1443 $[M + H]^+$	−1.494	Demethylation & glucuronidation of PMF **10**	S, L, C
M48	17.45	405.1185 $[M + H]^+$	$C_{20}H_{21}O_9$	405.1179 $[M + H]^+$	−1.481	Demethylation of PMF **11**	F, C
M49	17.53	551.1400 $[M + H]^+$	$C_{25}H_{27}O_{14}$	551.1393 $[M + H]^+$	−1.27	Demethylation & glucuronidation of PMF **9**	U, F, S, L
M50	17.6	375.1079 $[M + H]^+$	$C_{19}H_{19}O_8$	375.1074 $[M + H]^+$	−1.332	Demethylation of PMF **9**	U, F, S, C, G
M51	17.62	497.0753 $[M - H]^-$	$C_{21}H_{21}SO_{12}$	497.0758 $[M - H]^-$	1.005	Sulfation of PMF **11**	U, F, S, L, C
M52	17.65	359.1130 $[M + H]^+$	$C_{19}H_{19}O_7$	359.1124 $[M + H]^+$	−1.67	Demethylation of PMF **1**	U, F, S, C
M53	17.68	467.0648 $[M - H]^-$	$C_{20}H_{19}SO_{11}$	467.0652 $[M - H]^-$	0.856	Demethylation & sulfation of PMF **3**	U
M54	17.85	419.1342 $[M + H]^+$	$C_{21}H_{23}O_9$	419.1335 $[M + H]^+$	−1.67	Demethylation of PMF **5**	S
M55	17.91	405.1185 $[M + H]^+$	$C_{20}H_{21}O_9$	405.1179 $[M + H]^+$	−1.481	Demethylation of PMF **11**	F, C
M56	17.94	595.1663 $[M + H]^+$	$C_{27}H_{31}O_{15}$	595.1655 $[M + H]^+$	−1.344	Demethylation & glucuronidation of PMF **5**	U, S, L
M57	17.98	375.1079 $[M + H]^+$	$C_{19}H_{19}O_8$	375.1074 $[M + H]^+$	−1.332	Demethylation of PMF **8**	U, F, C, T
M58	18.01	359.1130 $[M + H]^+$	$C_{19}H_{19}O_7$	359.1125 $[M + H]^+$	−1.392	Demethylation of PMF **6**	U, F, P, S, L, C
M59	18.01	467.0648 $[M - H]^-$	$C_{20}H_{19}SO_{11}$	467.0645 $[M - H]^-$	−0.642	Demethylation & sulfation of PMF **3**	U
M60	18.28	405.1185 $[M + H]^+$	$C_{20}H_{21}O_9$	405.1179 $[M + H]^+$	−1.481	Demethylation of PMF **11**	U, F, C, T
M61	18.38	389.1236 $[M + H]^+$	$C_{20}H_{21}O_8$	389.1228 $[M + H]^+$	−2.055	Demethylation of PMF **3**	U, F, S, L, C
M62	18.47	359.1130 $[M + H]^+$	$C_{19}H_{19}O_7$	359.1125 $[M + H]^+$	−1.392	Demethylation of PMF **1**	U, F, P, S
M63	18.5	329.1025 $[M + H]^+$	$C_{18}H_{17}O_6$	329.1019 $[M + H]^+$	−1823	Demethylation of PMF **4**	U, F, P, S, L, C
M64	18.73	453.0491 $[M - H]^-$	$C_{19}H_{17}SO_{11}$	453.0502 $[M - H]^-$	2.427	Demethylation & sulfation of PMF **9**	F
M65	18.91	359.1130 $[M + H]^+$	$C_{19}H_{19}O_7$	359.1124 $[M + H]^+$	−1.67	Demethylation of PMF **10**	U, F, S, L, C, K
M66	19.32	359.1130 $[M + H]^+$	$C_{19}H_{19}O_7$	359.1124 $[M + H]^+$	−1.67	Demethylation of PMF **1**	U, F, S, L, C, K
M67	19.35	389.1236 $[M + H]^+$	$C_{20}H_{21}O_8$	389.1228 $[M + H]^+$	−2.055	Demethylation of PMF **3**	U, F, P, S, L, C, T
M68	19.72	389.1236 $[M + H]^+$	$C_{20}H_{21}O_8$	389.1227 $[M + H]^+$	−2.312	Demethylation of PMF **3**	U, F, P, S, L, C, K, T
M69	19.78	419.1342 $[M + H]^+$	$C_{21}H_{23}O_9$	419.1335 $[M + H]^+$	−1.67	Demethylation of PMF **5**	U, F, S
M70	20.18	419.1342 $[M + H]^+$	$C_{21}H_{23}O_9$	419.1333 $[M + H]^+$	−2.147	Demethylation of PMF **5**	U, F, P, S, L, C, K
M71	20.21	373.1287 $[M + H]^+$	$C_{20}H_{21}O_7$	373.1275 $[M + H]^+$	−3.216	PMF **1**	U, F, P, S, C, T
M72	20.41	373.1287 $[M + H]^+$	$C_{20}H_{21}O_7$	373.1275 $[M + H]^+$	−3.216	PMF **10**	F, S, L, C, B
M73	20.45	359.1130 $[M + H]^+$	$C_{19}H_{19}O_7$	359.1124 $[M + H]^+$	−1.670	Demethylation of PMF **10**	U, F, P, L
M74	20.73	403.1392 $[M + H]^+$	$C_{21}H_{23}O_8$	403.1383 $[M + H]^+$	2.232	PMF **2**	F, S, C
M75	21.02	375.1079 $[M + H]^+$	$C_{19}H_{19}O_8$	375.1074 $[M + H]^+$	−1.332	Demethylation of PMF **9**	U, F, P, S, C, T
M76	21.12	403.1392 $[M + H]^+$	$C_{21}H_{23}O_8$	403.1382 $[M + H]^+$	−2.480	PMF **3**	U, F, P, S, L, C, K
M77	21.32	343.1181 $[M + H]^+$	$C_{19}H_{19}O_6$	343.1170 $[M + H]^+$	−3.205	PMF **4**	U, F, P, S, L, C, T
M78	21.46	359.1130 $[M + H]^+$	$C_{19}H_{19}O_7$	359.1125 $[M + H]^+$	−1.392	Demethylation of PMF **6**	U, F, P
M79	21.52	375.1079 $[M + H]^+$	$C_{19}H_{19}O_8$	375.1074 $[M + H]^+$	−1.332	Demethylation of PMF **9**	U, F, P, S, C, T
M80	21.6	433.1498 $[M + H]^+$	$C_{25}H_{25}O_9$	433.1487 $[M + H]^+$	−2.539	PMF **5**	U, F, P, S, L, C
M81	22.41	403.1392 $[M + H]^+$	$C_{21}H_{23}O_8$	403.1382 $[M + H]^+$	−2.480	PMF **7**	F
M82	22.6	373.1287 $[M + H]^+$	$C_{20}H_{21}O_7$	373.1276 $[M + H]^+$	−2.948	PMF **6**	U, F, P, S, L, C, K, B
M83	22.77	389.1236 $[M + H]^+$	$C_{20}H_{21}O_8$	389.1225 $[M + H]^+$	−2.826	PMF **8**	U, F, P, S, L, C, K, T
M84	23.06	359.1130 $[M + H]^+$	$C_{19}H_{19}O_7$	359.1125 $[M + H]^+$	−1.392	Demethylation of PMF **6**	U, F, P, S, C, K
M85	23.59	359.1130 $[M + H]^+$	$C_{19}H_{19}O_7$	359.1125 $[M + H]^+$	−1.392	Demethylation of PMF **6**	U, F, P, S, C
M86	23.62	389.1236 $[M + H]^+$	$C_{20}H_{21}O_8$	389.1225 $[M + H]^+$	−2.826	PMF **9**	U, F, P, S, L, C, T
M87	23.92	389.1236 $[M + H]^+$	$C_{20}H_{21}O_8$	389.1228 $[M + H]^+$	−2.055	Demethylation of PMF **3**	U, F, S, L, C

colon-peel ratio, suggesting they may be more effectively absorbed or have a specific affinity for colon tissue. In terms of chemical properties, these two compounds do not contain a methoxy group at C-5. This absence may be a key factor in their enhanced accumulation in the colon.

3.6. Liver

Seven PMFs (**3**, **4**, **5**, **6**, **8**, **9**, and **10**) were detected in the liver. Among the non-hydroxylated PMFs, PMF **10** showed the highest liver-peel ratio followed by PMF **3**. Of the three hydroxylated PMFs, only PMFs **8** and **9** were detected, and they had a significantly higher liver-peel ratio than non-hydroxylated PMFs. However, the hydroxylated PMF **11** was not detected. Its unique structure, with methoxy groups at both the C-3 and C-6 positions, which are adjacent to the intramolecular hydrogen bond region (C-5 hydroxyl group and C-4 ketone group), may have influenced its accumulation. In contrast, PMF **8** lacks a methoxy group at the C-3 position, and PMF **9** lacks a methoxy group at the C-6 position. This suggests a potential chemical interaction between the hydrogen bond and its neighboring methoxy groups, an area that warrants future investigation. It is unlikely that the presence of PMF **8** is due to the demethylation of PMF **3**. The C-5 position is not considered an active site for demethylation, meaning only a small amount of PMF **3** would be metabolized into PMF **8**.

3.7. Kidney

Only three PMFs were detected in the kidney: two major PMFs (**3** and **6**) and one hydroxylated PMF (**8**). PMFs **3** and **6** have similar structure, with the methoxy groups at all positions on the A-ring and at the C-4′ position on the B-ring, but not on the C-ring. These two PMFs also showed a higher urine–peel ratio, approximately two times higher than other non-hydroxylated PMFs. These results can be attributed to two main factors. First, the lipophilicity of these PMFs leads to their primary excretion *via* feces. Second, due to their lipophilicity and molecular size, most PMFs are less likely to undergo reabsorption by the renal tubules. While studies on other flavonoid types have shown that tubular reabsorption is largely dependent on interactions with specific organic anion transporters like OAT1 and OAT3, no such transporters have been identified for PMFs.[31] Future investigations should aim to elucidate the specific reabsorption mechanisms of PMFs in the kidneys.

3.8. Enterohepatic recirculation

Among the major PMFs, PMF **3** had the highest ratio in feces, kidney, plasma, and liver, which suggested the enterohepatic recirculation. This process allows PMF **3** or its metabolites to be recycled between the intestine and the liver, prolonging their presence in the body and leading to higher concentrations in these organs. In contrast, only modest levels of PMF **3** were detected in the small intestine and colon, suggesting that it is efficiently absorbed into the bloodstream from the gastrointestinal tract, leaving lower amounts in the intestinal lumen. The high concentration of PMF **3** in plasma further supports this conclusion. Additionally, the presence of high concentrations of the parent compound indicates that PMF **3** is stable and remains largely unmetabolized, allowing for its direct

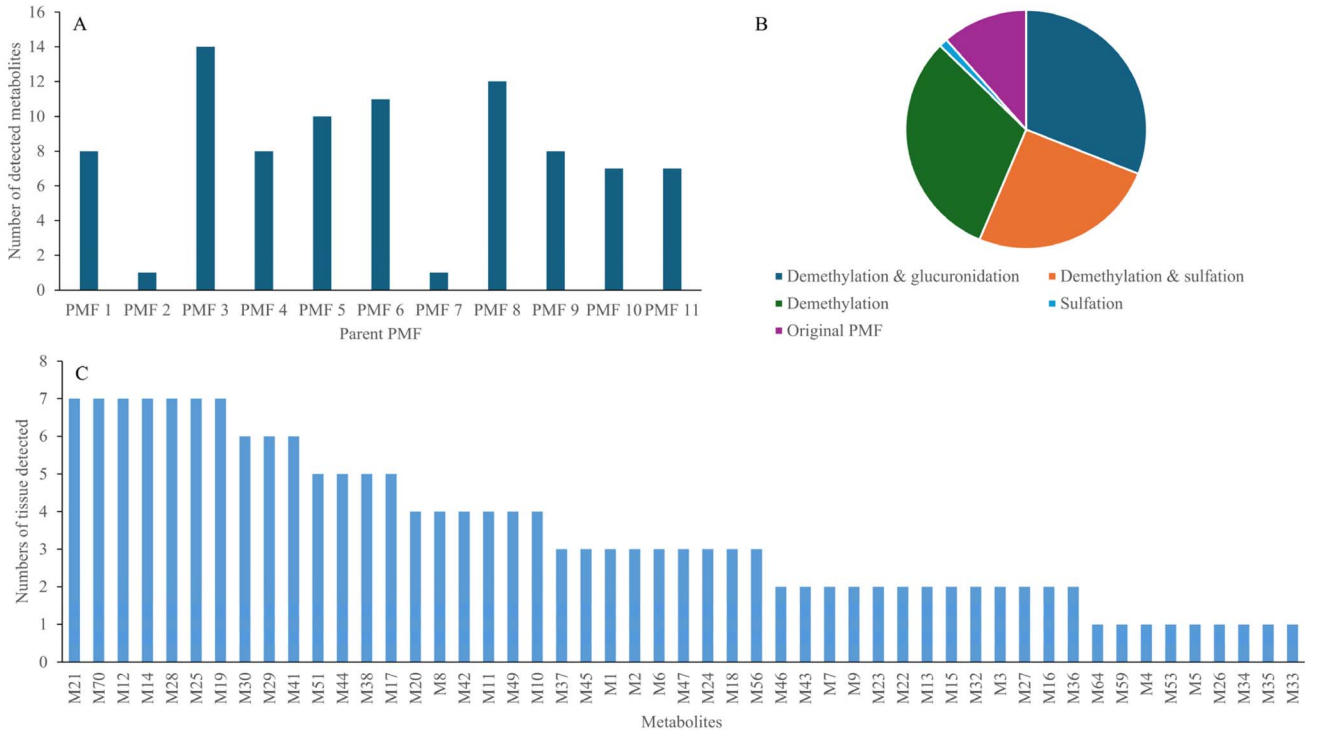

Fig. 3 Number of metabolites derived from each parent PMF (A); distribution of metabolites by metabolic pathway (B); distribution of PMF metabolites across tissues (C).

absorption. This direct absorption is highly beneficial for its bioavailability and therapeutic potential. It enhances the compound's efficacy, potentially allowing for lower dosages to achieve the desired therapeutic effects. This, in turn, may reduce side effects and improve patient compliance while also diminishing the compound's reliance on the enzymatic activity of the gastrointestinal tract.

3.9. PMF metabolites analysis

As shown in Table 3 and Fig. 3A, a total of 87 PMF metabolites (M1–M87) were detected in mice after the administration of orange peel extract. The data reveals the extensive metabolism of PMFs primarily through three key pathways: demethylation & glucuronidation, demethylation & sulfation, and simple demethylation (Fig. 3B). Demethylation and glucuronidation is the most common pathways, accounting for many the detected metabolites (*e.g.*, M6–M17, M19–M21, M23–M28, M32, M42, M45, M47, M49, M56). These metabolites are found across a wide variety of tissues. Demethylation & sulfation is also a significant pathway, contributing to a wide range of metabolites (*e.g.*, M1–M5, M18, M22, M29, M33–M38, M41, M43, M44, M46, M51, M53, M59, M64). Additionally, many metabolites (*e.g.*, M31, M39, M40, M48, M50, M52, M54, M55, M57, M58, M60-M63, M66, M69, M70, M73, M75, M78, M79, M84, M85, M87) were produced solely through demethylation. Metabolites from 11 PMFs were identified, with PMF **3** and PMF **8** appearing to be the most extensively metabolized. The identification of some representative metabolites was presented in Fig. 4. In a mass spectrum, as shown in Fig. 4A, the metabolite M21 (a glucuronate conjugate of PMF **6**) had a precursor ion at *m*/*z* 535.1443 in positive mode. This indicated the attachment of a glucuronate moiety ($C_6H_{10}O_7$) to parent pentamethoxyflavone. The product ion peak at *m*/*z* 373.1281 corresponded to the original pentamethoxyflavone, which has the molecular formula $C_{20}H_{21}O_7$. A subsequent product ion at *m*/*z* 351.0862 ($C_{17}H_{15}O_6$) was likely formed by the loss of one methoxy group and one methyl group, along with the cleavage of the C-1 to C-9 single carbon bond-a common fragmentation pattern in the flavonoid backbone.[32] Fig. 4B displayed the mass spectrum of M58, a sulfate conjugate of PMF **11**. The precursor ion appeared at *m*/*z* 497.0758, corresponding to the molecular formula $C_{21}H_{21}SO_{12}$. This ion can be explained by the attachment of sulfate (SO_4) to a hexamethoxy-one-hydroxy flavone compound.

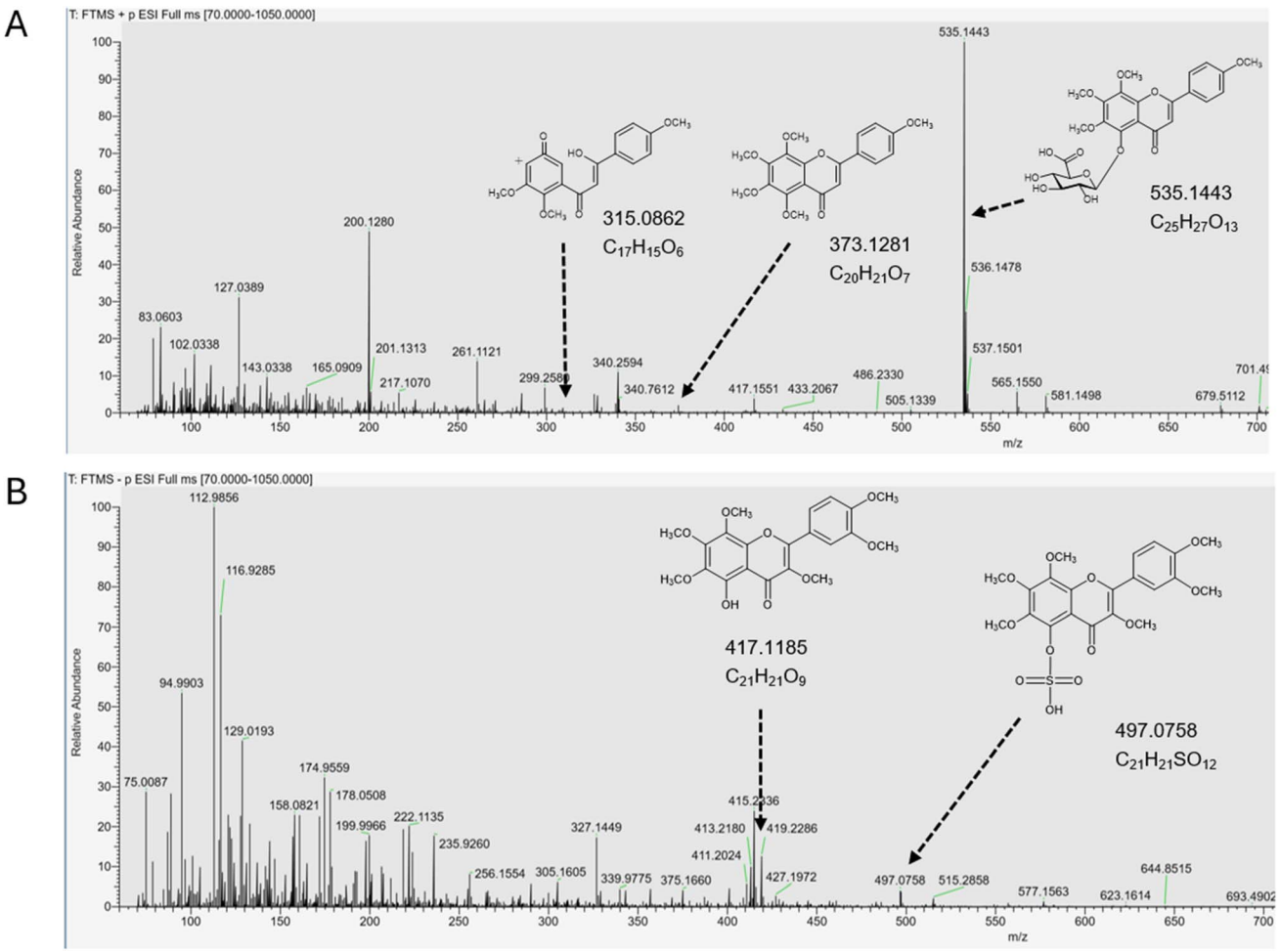

Fig. 4 Mass spectra of glucuronate conjugate and sulfate conjugate metabolites. (A) Glucuronate conjugate of PMF **6**, namely M21. Precursor ion appeared at *m*/*z* 535.1443. (B) Sulfate conjugate of PMF **11**, namely M58. Precursor ion appeared at *m*/*z* 497.0758.

The product peak at *m*/*z* 417.1185 suggested the original compound with the chemical formula $C_{21}H_{21}O_4$.

Among these metabolites, demethylated products were the most frequently found. The absence of hydroxyl groups in PMFs, which typically serve as attachment points for sulfate and glucuronate groups, makes demethylation a predominant transformation pathway. Meanwhile, a significant amount of demethylated metabolites were quantified after administration of sinensetin or nobiletin, identifying the C-4′ position as the most active site.[14,33] However, an *in vitro* study identified the C-3′ position as the most active site for demethylation.[34] Further analysis is needed to have a better understanding of PMF demethylation. Beyond the metabolic transformations, the data revealed a broad tissue-specific distribution of these compounds. Many metabolites, such as M14, M19, M21, and M70, were widely distributed, found in up to seven different tissues, including the liver and intestine which are crucial for metabolism (Fig. 3C). A particularly significant finding was the unique presence of certain compounds in less-common tissues, including the brain and testes, which pointed to their potential relevance for neuro- and reproductive health. Glucuronate and sulfate conjugation of PMFs were most commonly found in urine. These processes add polar groups to the compounds, increasing their water solubility and thereby facilitating their excretion *via* kidneys.

Our findings provide crucial translational insights into the *in vivo* bioavailability and tissue-specific distribution of naturally occurring PMFs from orange peel. The comprehensive analysis of 11 PMFs and their metabolites across various tissues is a significant step toward understanding their potential health benefits. The observed tissue-specific accumulation—for example, the presence of certain PMFs and their demethylated metabolites in the brain and testes—suggests that these compounds may have a role in organs not typically associated with classic PMF antioxidant or anti-inflammatory effects. This mechanistic understanding is highly relevant for the development of functional foods and therapeutic formulations. By knowing which PMFs have the highest bioavailability and where they accumulate, formulators can design more effective products. For instance, a formulation targeting brain health might be enriched with PMFs that show a greater ability to cross the BBB. Similarly, understanding the metabolic pathways (glucuronidation, sulfation, demethylation) allows for the prediction of how these compounds will be processed in the body, which is essential for determining optimal dosing and predicting potential interactions. While our study was conducted in a mouse model, detailed *in vivo* data provided a strong scientific foundation that can guide future human clinical trials. Ultimately, our work helps bridge the gap between *in vitro* studies and applications, paving the way for the rational design of orange peel-based nutraceuticals with targeted health benefits.

4. Conclusions

To understand PMF metabolism and distribution, mice were orally administered orange peel extract, and PMF levels in different tissues were analyzed using LC-MS. The concentration of parent PMFs was quantified in both the orange peel and various tissues, which allowed us to correlate chemical structures with bioavailability. Using key-ion patterns, we identified the original compounds from which the metabolites were derived. This study is the first to report on the practical distribution of PMFs after oral administration of a natural orange peel extract. We believe these findings provide a new perspective on the complex metabolism of PMFs and reinforce their potential as nutraceuticals.

Author contributions

Jin-Pyo An: formal analysis, writing – original draft. Xin Liu: investigation. Dongjoo Kim: resources. Robert Madden: methodology. Yu Wang: conceptualization, project administration, writing – review and editing.

Conflicts of interest

The authors declare that they do not have competing interests.

Data availability

. Supplementary information: optimal MS/MS parameters for quantiva analysis; linearity, LOD, and LOQ for polymethoxyflavones; precision and recovery values for polymethoxyflavones; recovery rates for each tissue; parameters for Orbitrap high-resolution mass spectrometry; the tissue-to-peel ratio (calculated as the percentage obtained by dividing the content of each PMF in a specific tissue by its content in orange peel); chemical structures of the 11 polymethoxyflavones in orange peel; and the distribution of polymethoxyflavones across various tissues. See DOI: **https://doi.org/10.1039/d5ra03091a**.

Acknowledgements

This work was supported by the USDA National Institute of Food and Agriculture (Grant Number 2018-07925).

References

1 Q. Chen, Y. Gu, C. Tan, B. Sundararajan, Z. Li, D. Wang and Z. Zhou, *Front. Nutr.*, 2022, **9**, e963662.
2 J. H. Yen, C. Y. Weng, S. Li, Y. H. Lo, M. H. Pan, S. H. Fu, C. T. Ho and M. J. Wu, *Mol. Nutr. Food Res.*, 2011, **55**, 733–748.
3 C. S. Lai, M. H. Ho, M. L. Tsai, S. Li, V. Badmaev, C. T. Ho and M. H. Pan, *J. Agric. Food Chem.*, 2013, **61**, 10320–10328.
4 M. S. Shajib, R. B. Rashid, L. C. Ming, S. Islam, M. M. R. Sarker, L. Nahar, S. D. Sarker, B. K. Datta and M. A. Rashid, *Front. Pharmacol*, 2018, **9**, e85.
5 M. H. Pan, M. Y. Li, M. L. Tsai, C. Y. Pan, V. Badmaev, C. T. Ho and C. S. Lai, *Food Funct.*, 2019, **10**, 7667–7677.
6 C. Yang, H. Chen, H. Chen, B. Zhong, X. Luo and J. Chun, *Molecules*, 2017, **22**, e1391.

7 A. Gosslau, K. Y. Chen, C. T. Ho and S. Li, *Food Sci. Hum. Wellness*, 2014, **3**, 26–35.
8 T. Walle, *Mol. Pharmaceutics*, 2007, **4**, 826–832.
9 C. T. Ho, J. Simon, F. Shahidi and Y. Shao, in *Polymethoxyflavones: Metabolite Identification and Pathway*, American Chemical Society, Washington, D.C, 2008, vol. 1, pp. 216–232, DOI: **10.1021/bk-2008-0987.ch015**.
10 C. Manach and J. L. Donovan, *Free Radical Res.*, 2004, **38**, 771–786.
11 X. Wen and T. Walle, *Drug Metab. Dispos.*, 2006, **34**, 1786–1792.
12 T. Walle, N. Ta, T. Kawamori, X. Wen, P. A. Tsuji and U. K. Walle, *Biochem. Pharmacol.*, 2007, **73**, 1288–1296.
13 P. Hodek, P. Trefil and M. Stiborová, *Chem.-Biol. Interact.*, 2002, **139**, 1–21.
14 X. Wang, D. Li, Y. Cao, C. T. Ho and Q. Huang, *J. Agric. Food Chem.*, 2021, **69**, 14143–14150.
15 W. L. Hung, W. S. Chang, W. C. Lu, G. J. Wei, Y. Wang, C. T. Ho and L. S. Hwang, *J. Food Drug Anal.*, 2018, **26**, 849–857.
16 M. Iwashita, R. Shioi, M. Sugiyama, K. Hashizume, T. Kan, S. Naito, H. Takai, Y. Kawase, T. Hamabe-Horiike, Y. Katanasaka and Y. Sunagawa, *J. Agric. Food Chem.*, 2023, **71**, 10028–10036.
17 H. Lee, X. Liu, J. P. An and Y. Wang, *J. Agric. Food Chem.*, 2023, **71**, 16114–16124.
18 H. Lee, G. Y. Koh, H. Lee, P. Alves, W. Yokoyama and Y. Wang, *J. Agric. Food Chem.*, 2024, **72**, 7870–7881.
19 G. R. Velderrain-Rodríguez, H. Palafox-Carlos, A. Wall-Medrano, J. F. Ayala-Zavala, C. O. Chen, M. Robles-Sánchez, H. Astiazaran-García, E. Alvarez-Parrilla and G. A. González-Aguilar, *Food Funct.*, 2014, **5**, 189–197.
20 Z. Chen, S. Zheng, L. Li and H. Jiang, *Curr. Drug Metab.*, 2014, **15**, 48–61.
21 G. Borges, J. I. Ottaviani, J. J. van der Hooft, H. Schroeter and A. Crozier, *Mol. Aspects Med.*, 2018, **61**, 18–30.
22 F. Cuyckens and M. Claeys, *J. Mass Spectrom.*, 2004, **39**, 1–15.
23 M. Zhang, Y. Xin, K. Feng, B. Yin, Q. Kan, J. Xiao, Y. Cao, C. T. Ho and Q. Huang, *J. Agric. Food Chem.*, 2020, **68**, 10709–10718.
24 A. Murakami, S. Kuwahara, Y. Takahashi, C. Ito, H. Furukawa, M. Ju-ichi, K. Koshimizu and H. Ohigashi, *Biosci. Biotechnol. Biochem.*, 2001, **65**, 194–197.
25 D. G. Goulis and B. C. Tarlatzis, *Gynecol. Endocrinol.*, 2008, **24**, 33–39.
26 H. J. Lee, S. K. Lee, D. R. Lee, B. K. Choi, B. Le and S. H. Yang, *Mol. Med. Rep.*, 2019, **20**, 3448–3455.
27 M. Al Rahim, A. Nakajima, D. Saigusa, N. Tetsu, Y. Maruyama, M. Shibuya, H. Yamakoshi, Y. Tomioka, Y. Iwabuchi, Y. Ohizumi and T. Yamakuni, *Biochemistry*, 2009, **48**, 7713–7721.
28 J. Y. Yoo, M. Groer, S. V. O. Dutra, A. Sarkar and D. I. McSkimming, *Microorganisms*, 2020, **8**, 1587.
29 M. Zhang, J. Zhu, X. Zhang, D. G. Zhao, Y. Y. Ma, D. Li, C. T. Ho and Q. Huang, *Food Funct.*, 2020, **11**, 2667–2678.
30 J. Chen, Y. Wang, T. Zhu, S. Yang, J. Cao, X. Li, L. S. Wang and C. Sun, *Antioxidants*, 2020, **9**, 831.
31 C. C. Wong, N. P. Botting, C. Orfila, N. Al-Maharik and G. Williamson, *Biochem. Pharmacol.*, 2011, **81**, 942–949.
32 C. M. Sawicki, D. L. McKay, N. M. McKeown, G. Dallal, C. Y. O. Chen and J. B. Blumberg, *Nutrients*, 2016, **8**, e813.
33 L. Li, Y. Chen, X. Feng, J. Yin, S. Li, Y. Sun and L. Zhang, *Molecules*, 2019, **24**, e2658, DOI: **10.3390/molecules24142658**.
34 Q. You, D. Li, H. Ding, H. Chen, Y. Hu and Y. Liu, *J. Agric. Food Chem.*, 2021, **69**, 12705–12716.